INTERNATIONAL JOURNAL FOR NUMERICAL METHODS IN FLUIDS, VOL. 25, 495–512 (1997)

COMPUTER-AIDED ANALYSIS OF FLOW PAST A SURFACE-MOUNTED OBSTACLE

V. P. FRAGOS,[1] S. P. PSYCHOUDAKI[1] AND N. A. MALAMATARIS[2]*

[1] *Department of Hydraulics, Soil Sciences and Agricultural Engineering, Aristotle University of Thessaloniki, GR-54006 Thessaloniki, Greece*

[2] *Department of Chemical Engineering, University Box 453, Aristotle University of Thessaloniki, Box 453, GR-54006 Thessaloniki, Greece*

SUMMARY

The incompressible, laminar, isothermal flow of a Newtonian fluid at steady state past a surface-mounted obstacle (flow over a step) is studied in a two-dimensional numerical experiment using the Galerkin finite element method. The dimensionless Navier–Stokes equations are solved in the whole range of the laminar flow regime. The numerical predictions are compared with available experimental data. The emphasis in the discussion of the results is on the presentation of the streamlines for various Reynolds numbers, the pressure distribution over and downstream of the step, the shear stress distribution along the surface of the step and the length of the recirculation region as a function of the Reynolds number. This analysis may be used in numerous applications from agricultural to civil, mechanical and chemical engineering. © 1997 by John Wiley & Sons, Ltd.

Int. J. Numer. Meth. Fluids, **25**: 495–512 (1997).

No. of Figures: 22. No. of Tables: 2. No. of References: 37.

KEY WORDS: separated flows; recirculation length; finite element method

1. INTRODUCTION

The flow over a surface-mounted obstacle is a combination of the flow over a forward- and backward-facing step. This flow is considered a good prototype for numerous applications in industry, including the study of air pollution, power plant location, wind loading on tall buildings,[1,2] turbomachines,[3] car aerodynamics,[4] cooling of electronic equipment and gas-cooled reactors,[5] meteorology and wind energy applications,[6] flow over road embankments and modern architectural buildings[7] and design of fluid-handling devices.[8] In addition, the two elementary components of this flow, the forward- and the backward-facing step, are quite often used as test cases for new developments in numerical algorithms,[9–11] in outflow boundary conditions[12–14] and in answering fundamental questions of computational interest regarding these flows.[15].

In the numerical study of turbulent flow over a surface-mounted obstacle, there have been numerous attempts to solve the problem using the standard k–ε model and various modifications of it, with partial success considering the comparisons of numerical predictions with experimental results.[16–20] Apart from the inaccuracy of the turbulence models due to the incomplete understanding

* Correspondence to: N. A. Malamataris, Department of Chemical Engineering, University Box 453, Aristotle University of Thessaloniki, GR-54006, Thessaloniki, Greece.

CCC 0271–2091/97/050495–18 $17.50
© 1997 by John Wiley & Sons, Ltd.
Received 27 November 1995
Revised 7 October 1996

of turbulence, the discrepancy between numerical solutions and experimental data is also attributed to reasons common to both laminar and turbulent models, such as the structure and refinement of the mesh,[16] the height of the upper boundary and the appropriate boundary condition there,[1,9] upstream conditions[1] and the still open-ended issue of outflow boundary conditions.[14,21]

In the numerical study of laminar flow over a surface-mounted obstacle, early attempts to solve the problem have been made by Greenspan[22] and Friedman[23] using finite differences. Later work by Leone and Gresho[24] represents still the most accurate numerical simulations reported to date. The primary objective though of Leone and Gresho was to demonstrate that the conventional Galerkin finite element method is to be preferred in the solution of complex non-linear flow problems over recent upwind schemes. Therefore there is a lack of comparison of their numerical experiments with available experimental data of Taneda[25] and Acrivos *et al.*[26] in the laminar flow regime.

This work has been motivated by the need to calculate the pressure distribution of air along the sides of greenhouses in agricultural engineering applications for a wide range of Reynolds numbers. The flow problem has been approached from the viewpoint of the numerical analyst who aims at the design of numerical experiments in order to supplement physical experiments in the understanding of the flow phenomena around surface-mounted obstacles. The computational domain has thus been chosen in such a way as to resemble actual wind tunnel experiments, as described in the next section. In this way, shortcomings of previous numerical analyses regarding upstream conditions, location of the upper boundary, etc. are alleviated.

The methodology of the work was to start by computing the limit of Stokes flow, then advance to higher Reynolds numbers and check the numerical experiments with corresponding physical ones and finally make predictions for this flow in the whole range of the laminar regime. In the next section the problem statement is described along with the governing equations for laminar flow and the appropriate boundary conditions (Section 2). The numerical method is then briefly explained (Section 3), the numerical predictions are presented, discussed and compared with available experimental data (Section 4) and finally conclusions are drawn (Section 5).

2. GOVERNING EQUATIONS AND BOUNDARY CONDITIONS

The computational domain for the flow over a surface-mounted obstacle is shown in Figure 1. A Newtonian fluid of constant density and viscosity approaches a closed wind tunnel with a uniform velocity u_0. At the entrance of the wind tunnel the fluid is decelerated along the wall owing to the no-slip boundary condition and it approaches the surface-mounted obstacle, which is a step. Around and in the vicinity of the obstacle, separation and reattachment of the flow occur and the fluid leaves the computational domain at a location where these flow phenomena gradually fade.

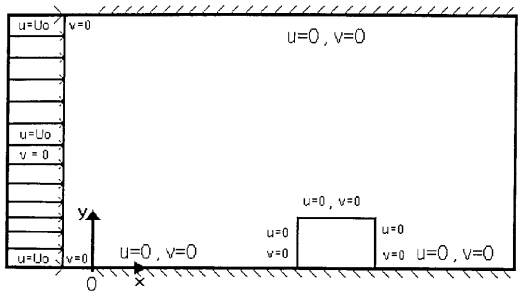

Figure 1. Computational domain for flow over a surface-mounted obstacle

 © 1997 by John Wiley & Sons, Ltd.

The flow is laminar, isothermal, incompressible, two-dimensional, at steady state and the dimensionless Navier–Stokes equations are

$$\nabla \cdot \mathbf{u} = 0, \tag{1}$$

$$\mathbf{u} \cdot \nabla \mathbf{u} = -\nabla p + \frac{1}{Re} \nabla^2 \mathbf{u}. \tag{2}$$

Equations (1) and (2) represent the conservation of mass (continuity equation) and momentum respectively. Here $\mathbf{u} = (u, v)$ is the velocity vector in the fluid, with u and v its components in the x- and y-direction respectively, p is the pressure and $Re = u_0 H/v$ is the Reynolds number, with u_0 the uniform approaching velocity of the fluid from the wind tunnel, H the height of the step and v the kinematic viscosity of the fluid. The pressure p has been non-dimensionalized with the magnitude ρu_0^2, with ρ the density of the fluid.

The boundary conditions for this flow are depicted in Figure 1:

$$\text{at the entrance} \quad \begin{cases} u = 1, & (3) \\ v = 0, & (4) \end{cases}$$

top and bottom boundaries

$$\text{upstream of the wind tunnel} \quad \begin{cases} u = 1, & (5) \\ v = 0, & (6) \end{cases}$$

$$\text{in the wind tunnel} \quad \begin{cases} u = 0, & (7) \\ v = 0, & (8) \end{cases}$$

$$\text{along the obstacle surface} \quad \begin{cases} u = 0, & (9) \\ v = 0, & (10) \end{cases}$$

at the outflow: free boundary condition.

Equations (3) and (4) impose a uniform freestream at the entrance of the computational domain. Along the top and bottom upstream of the tunnel, tow tank boundary conditions have been chosen (equations (5) and (6)). The no-slip boundary condition has been imposed along the top and bottom walls of the tunnel (equations (7) and (8)) and along the surface of the step (equations (9) and (10)). The free boundary condition has been applied at the outflow in order to let the fluid leave the computational domain freely without any distortion of the flow in the interior. The next section briefly outlines how this recent idea[13,27] is included in the formulation of the finite element method by evaluating the surface integral of equation (13). It is beyond the scope of this work to go into the details of its implementation, which can be found elsewhere,[28] or into its mathematical insight, which has, to a significant extent, been accomplished by Sani and Gresho[14] and Heinrich and Vionnet;[29] additional work on this subject can be found in References 30 and 31. However, a few runs are presented that check the validity of the free boundary condition along with the rest of the results of this work in Section 4.

3. FINITE ELEMENT FORMULATION

Two computational meshes that we believe guarantee mesh-independent solutions were used in this work and are shown in Figures 2 and 3 respectively. In Figure 2 the surface-mounted obstacle is a square of unit length in order to simulate the experiments of separated Stokes flow of Taneda[25] and to make predictions in the whole range of the laminar regime. In Figure 3 the surface-mounted obstacle

© 1997 by John Wiley & Sons, Ltd.

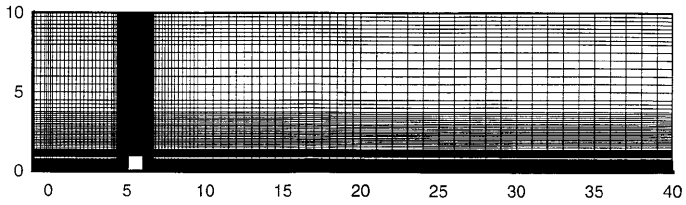

Figure 2. Mesh tesselation of computational domain for simulation of Taneda's experiment[25]

is a rectangle of width 0·45 and height 1 in order to simulate the experiments of Acrivos *et al.*[26]. The details of the two computational meshes are summarized in Tables I and II respectively.

The unknown velocities u and v and the pressure p of the governing equations (1) and (2) are expanded in terms of Galerkin basis functions as

$$u = \sum_{i=1}^{9} u_i \phi^i, \qquad v = \sum_{i=1}^{9} v_i \phi^i, \qquad p = \sum_{i=1}^{4} p_i \psi_i,$$

where ϕ^i are biquadratic and ψ^i bilinear basis functions. The governing equations, weighted integrally with the basis functions, resulted in the following continuity, R_{C}^i, and momentum, R_{M}^i, residuals:

$$R_{\mathrm{C}}^i = \int_V \nabla \cdot \mathbf{u} \psi^i \mathrm{d}V, \tag{11}$$

$$R_{\mathrm{M}}^i = \int_V \left[\mathbf{u} \cdot \nabla \mathbf{u} - \nabla \cdot \left(-p\mathbf{I} + \frac{1}{Re}\mathbf{T} \right) \right] \phi^i \mathrm{d}V. \tag{12}$$

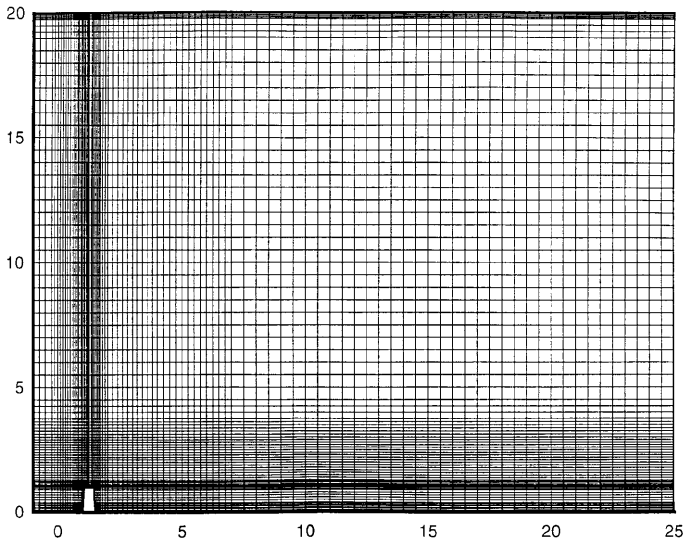

Figure 3. Mesh tesselation of computational domain for simulation of Acrivos *et al.*'s experiment[26]

 © 1997 by John Wiley & Sons, Ltd.

Table I. Data of computational mesh of Figure 2

Number of elements	11199
Number of nodes	45313
Number of unknowns	102084
Matrix front width	453
CPU time per iteration	40 min
Location of step	$5 \leqslant x \leqslant 6$
Height of step	$0 \leqslant y \leqslant 1$

x-co-ordinate of nodes

-1, $-0{\cdot}75$, $-0{\cdot}5$, $-0{\cdot}25$, $-0{\cdot}125$,0, 0·125, 0·25, 0·75, 1, 1·25, 1·5, 1·75, 2, 2·25, 2·5, 2·75, 3, 3·25, 3·5, 3·75, 4, 4·2, 4·3, 4·35, 4·4, 4·45, 4·5, 4·55, 4·6, 4·65, 4·7, 4·75, 4·8, 4·85, 4·9, 4·925, 4·95, 4·975, 5, 5·025, 5·05, 5·07, 5·1, 5·15, 5·2, 5·25, 5·3, 5·35, 5·4, 5·45, 5·5, 5·55, 5·6, 5·65, 5·7, 5·75, 5·8, 5·85, 5·9, 5·925, 5·95, 5·975, 6, 6·025, 6·05, 6·075, 6·1, 6·15, 6·2, 6·25, 6·3, 6·35, 6·4, 6·45, 6·5, 6·55, 6·6, 6·65, 6·7, 6·8, 7, 7·2, 7·4, 7·6, 7·8, 8, 8·25, 8·5, 8·75, 9, 9·25, 9·5, 10, 10·5, 11, 11·5, 12, 12·5, 13,. . ., 20, 21, 22, 23,. . ., 40

y-co-ordinate nodes

0, 0·005, 0·01, 0·015, 0·02, 0·025, 0·03, 0·04, 0·05, 0·06, 0·07, 0·08, 0·09, 0·1, 0·125, 0·15, 0·175, 0·2, 0·25, 0·3, 0·35, 0·4, 0·45, 0·5, 0·55, 0·6, 0·65, 0·7, 0·75, 0·8, 0·9, 0·925, 0·95, 0·975, 1, 1·01, 1·02, 1·03, 1·04, 1·06, 1·08, 1·1, 1·125, 1·15, 1·175, 1·2, 1·25, 1·3, 1·35, 1·4, 1·5, 1·6, 1·7, 1·8, 1·9, 2, 2·1, 2·2, 2·3, 2·4, 2·5, 2·6, 2·7, 2·8, 2·9· 3, 3·125, 3·25, 3·375, 3·5, 3·625, 3·75, 4, 4·25, 4·5, 5, 5·5, 6, 6·5, 7, 7·5, 8·25, 8·5, 8·75, 9, 9·25, 9·5, 9·75, 10

Table II. Data of computational mesh of Figure 3

Number of elements	8048
Number of nodes	32589
Number of unknowns	73425
Matrix front width	448
CPU time per iteration	20 min
Location of step	$1 \leqslant x \leqslant 1{\cdot}45$
Height of step	$0 \leqslant y \leqslant 1$

x-co-ordinate of nodes

-1, $-0{\cdot}75$, $-0{\cdot}5$, $-0{\cdot}25$, $-0{\cdot}125$, 0, 0·1, 0·2, 0·3, 0·4, 0·5, 0·6, 0·65, 0·7, 0·75, 0·8, 0·85, 0·9, 0·95, 1, 1·05, 1·10, 1·15, 1·2, 1·25, 1·35, 1·4, 1·45, 1·5, 1·55, 1·6, 1·65, 1·7, 1·8, 1·9, 2·2, 2·4, 2·8, 3, 3·2, 3·4, 3·6, 3·8, 4, 4·25, 4·5, 4·75, 5, 5·25, 5·5, 5·75, 6, 6·25, 6·75, 7, 7·5, 8, 8·5, 9, 9·5, 10, 10·5, 11, 11·5, 12, 12·5, 13, 13·5, 14, . . . , 25

y-co-ordinate of nodes

0, 0·025, 0·05, 0·075, 0·1, 0·15, 0·2, 0·25, 0·3, 0·35, 0·4, 0·5, 0·6, 0·7, 0·8, 0·9, 0·95, 1, 1·025, 1·05, 1·075, 1·1, 1·15, 1·2, 1·25, 1·3, 1·4, 1·5, 1·6, 1·7, 1·8, 1·9, 2, 2·1, 2·2, 2·3, 2·4, 2·5, 2·6, 2·7, 2·8, 2·9, 3, 3·125, 3·25, 3·375, 3·5, 3·625, 3·75, 4, 4·25, 4·5, 5, 5·5, 6, 6·5· 7, 7·7, 8, 8·5, 9, 9·5, 10·5, 11, . . . , 19, 19·25, 19·5, 19·75, 19·8, 19·85, 19·95, 20

© 1997 by John Wiley & Sons, Ltd.

Here $\mathbf{I}$ is the identity matrix and $\mathbf{T} = \nabla\mathbf{u} + (\nabla\mathbf{u})^{\mathrm{T}}$ is the stress tensor of the Newtonian fluid, with $\nabla^2\mathbf{u} = \nabla \cdot \mathbf{T}$ (equation (2)). By applying the divergence theorem in order to decrease the order of differentiation, equation (12) reduces to

$$R_{\mathrm{M}}^i = \int_V \left[(\mathbf{u} \cdot \nabla\mathbf{u})\phi^i - \left(-p\mathbf{I} + \frac{1}{Re}\mathbf{T} \right) \cdot \nabla\phi^i \right] \mathrm{d}V - \int_S \mathbf{n} \cdot \left(-p\mathbf{I} + \frac{1}{Re}\mathbf{T} \right) \phi^i \mathrm{d}S. \tag{13}$$

Since essential boundary conditions for u and v are applied to all boundaries of the domain except for the outflow, equation (13) will be replaced by equations (3)–(10). The inclusion of the surface integral of equation (13) along the outflow boundary of the domain is essentially the imposition of the free boundary condition in the FORTRAN-77 programme created by the authors for the computations of this work. Details on the programming strategy and the actual implementation of the free boundary condition for this problem can be found in Reference 32.

The residuals are evaluated numerically using nine-point Gaussian integration. A system of non-linear algebraic equations results, which is solved with the Newton–Raphson iterative method according to the scheme $\mathbf{q}^{(n+1)} = \mathbf{q} - \mathbf{J}^{-1}\mathbf{R}(\mathbf{q}^{(n)})$, where $\mathbf{q} = [u_1, v_1, p_1, \ldots, u_N, v_N, p_N]$ is the vector of the unknowns and $\mathbf{J} = \partial\mathbf{R}/\partial\mathbf{q}$ is the Jacobian matrix of the residuals $\mathbf{R}$ with respect to the nodal unknowns $\mathbf{q}$. The banded matrix of the resulting linear equations is solved with a frontal solver[33] at each iteration. The computer runs have been performed on a DEC OSF/1 V3.2-Alpha 7000-610 AXP of the Democritus University of Thrace. Zeroth-order continuation has been used as an initial guess to advance from one *Re* solution to another and the Newton procedure in all computer runs converged quadratically in four to six iterations.

4. RESULTS AND DISCUSSION

The simulation of Taneda's[25] experiment, of a separated Stokes flow, with the computational mesh of Figure 2 was the first computer run of this work. Figure 4 shows the calculated streamlines and a photograph taken from Taneda's experiments.[34] Figures 4(a) and 4(b) are by inspection identical. It can be clearly seen that the flow is symmetrical, with the same streamline patterns upstream and downstream of the obstacle. The separation points of the numerical predictions coincide with the experimental observations, as does the distance of the vortex centres from the corners of the obstacles.

The pressure and vorticity distributions of Figure 5, along with the streamline pattern in the whole computational domain, also display the parallel characteristic of Stokes flow in the vicinity of the step. At the entrance of the channel, strong generation of vorticity and steep pressure gradients are observed owing to the sudden deceleration of the fluid from the free stream velocity before the

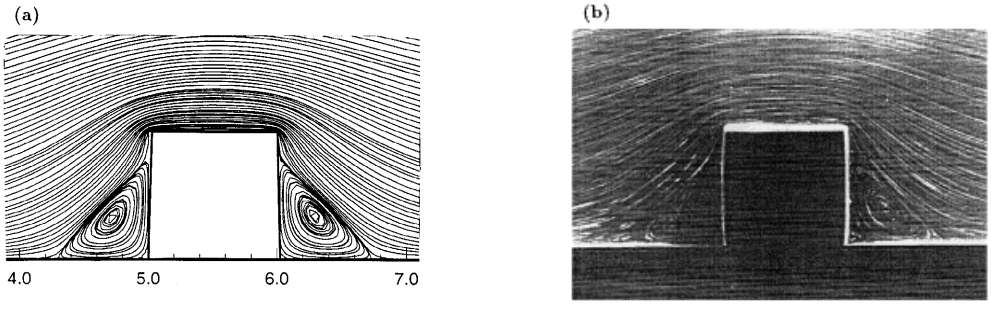

Figure 4. Separated Stokes flow around a surface-mounted obstacle: (a) numerical prediction of this work; (b) Taneda's experiment[25]

 © 1997 by John Wiley & Sons, Ltd.

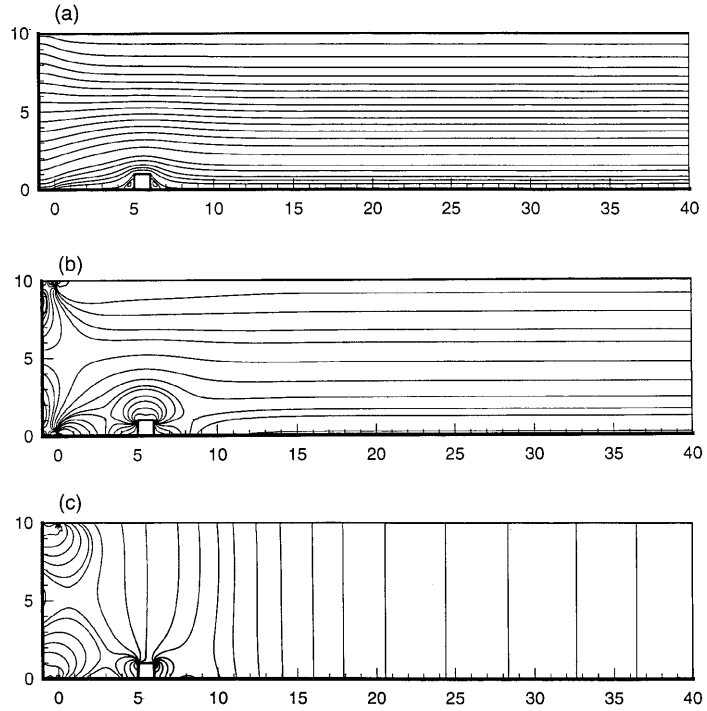

Figure 5. Separated Stokes flow around a surface-mounted obstacle: (a) streamline pattern; (c) pressure distribution (b) vorticity distribution

entrance to the no-slip boundary condition along the walls of the tunnel. The position of the obstacle 5 units downstream of the entrance permits both the entrance effects to fade gradually and the Stokes characteristics in the distribution of streamlines, vorticity and pressure to develop freely and undisturbed. A closer look at the distribution of pressure and vorticity in the vicinity of the obstacle is shown in Figure 6, where it is clearly demonstrated how sharp the changes are of both magnitudes in the corners of the obstacle and how symmetrically the isobars and vorticity contours develop with an axis of symmetry on a vertical line through the middle of the step.

Next the results of the simulations of Acrivos' *et al.* experiments[26] are shown in Figures 7–13. They measured the length of the recirculation region downstream of a rectangular step, the pressure distribution along the bottom of the tunnel downstream of the step and the velocity profiles in the recirculation region. Additionally, they showed a photograph with a typical streamline pattern at $Re = 70$. In Figures 7 and 8 the calculated streamlines of this work are shown for $0.1 \leqslant Re \leqslant 70$. The length and width of the recirculation region increase gradually with increasing Reynolds number. Figure 9 shows the effect of the Reynolds number on the recirculation length of the calculated streamline patterns along with the corresponding experimental measurements of Acrivos *et al.* The agreement between numerical and experimental data is within 27% at the lowest measured Reynolds number and the discrepancy diminishes to zero as the Reynolds number increases. Figure 10 shows the comparison of the calculated streamlines at $Re = 70$ with the photograph of Acrivos *et al.* (Reference 26, p. 48). The numerical and experimental streamline patterns coincide in the length and shape of the recirculation region but exhibit a discrepancy in the location of the vortex centre. Since the experiments performed by Acrivos *et al.* were in the opposite direction to our analysis, for this particular case the x-co-ordinate of the computed results in the plotter programme was reversed in

© 1997 by John Wiley & Sons, Ltd.

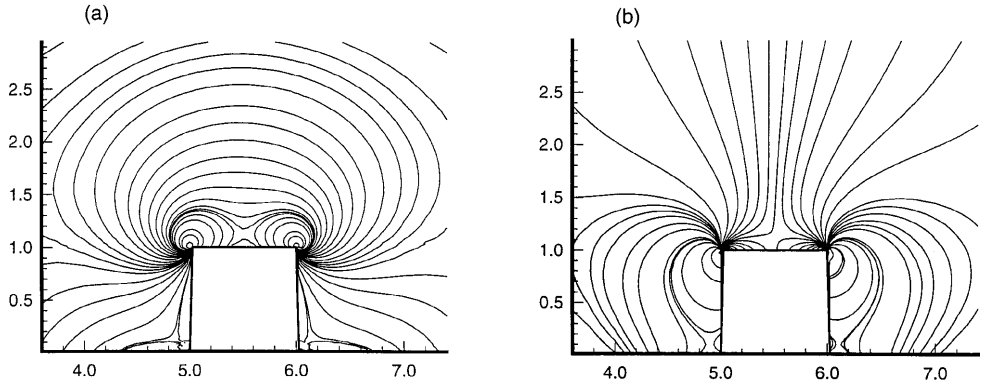

Figure 6. Separated Stokes flow around a surface-mounted obstacle: closer look at (a) vorticity and (b) pressure distributions

order to facilitate the comparison with the experiment. Typical u-velocity profiles for the flow field of Figure 10 are shown in Figure 11 at four different locations along the tunnel with the corresponding profiles of the flow in the absence of the step. The velocity profiles in the empty tunnel are, as expected, symmetrical, while the corresponding ones in the presence of the step exhibit an acceleration due to the blockage effect of the step, which is most pronounced in Figures 11(b) and 11(c) which were taken on the step and in the recirculation region downstream respectively. As the flow approaches the top of the tunnel, the velocity profiles with and without the presence of the step become identical—apart from Figure 11(d) where the flow rearranges itself to channel flow—

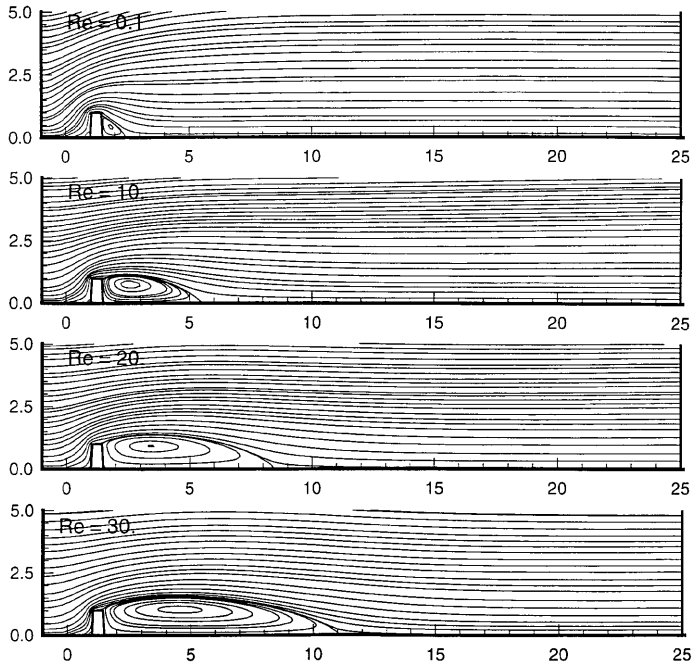

Figure 7. Numerical predictions of streamline patterns for flow over a rectangular step for $0{\cdot}1 \leqslant Re \leqslant 30$

 © 1997 by John Wiley & Sons, Ltd.

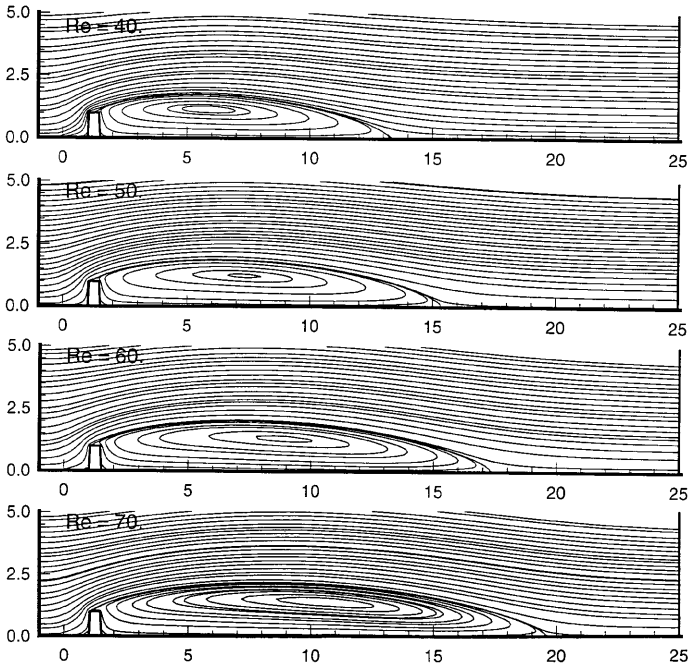

Figure 8. Numerical predictions of streamline patterns for flow over a rectangular step for $40 \leqslant Re \leqslant 70$

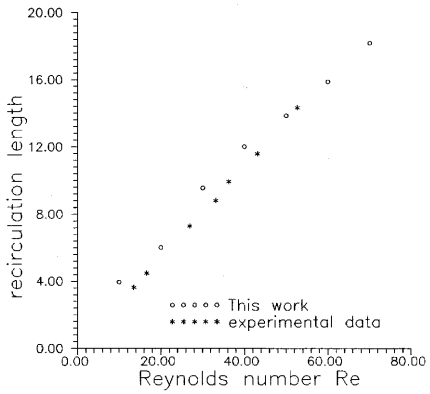

Figure 9. Comparison of numerical predictions of this work with experimental data of Acrivos *et al.* for length of recirculation region in limit of high Reynolds numbers for flow over a rectangular step

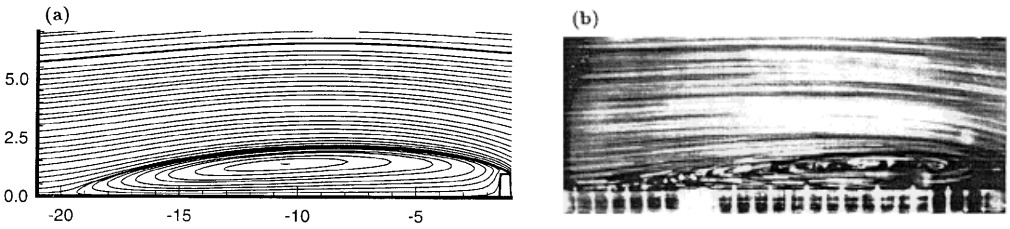

Figure 10. Comparison of (a) numerical predictions of this work with (b) experimental data of Acrivos *et al.* for streamline patterns at $Re = 70$ for flow over a rectangular step

© 1997 by John Wiley & Sons, Ltd.

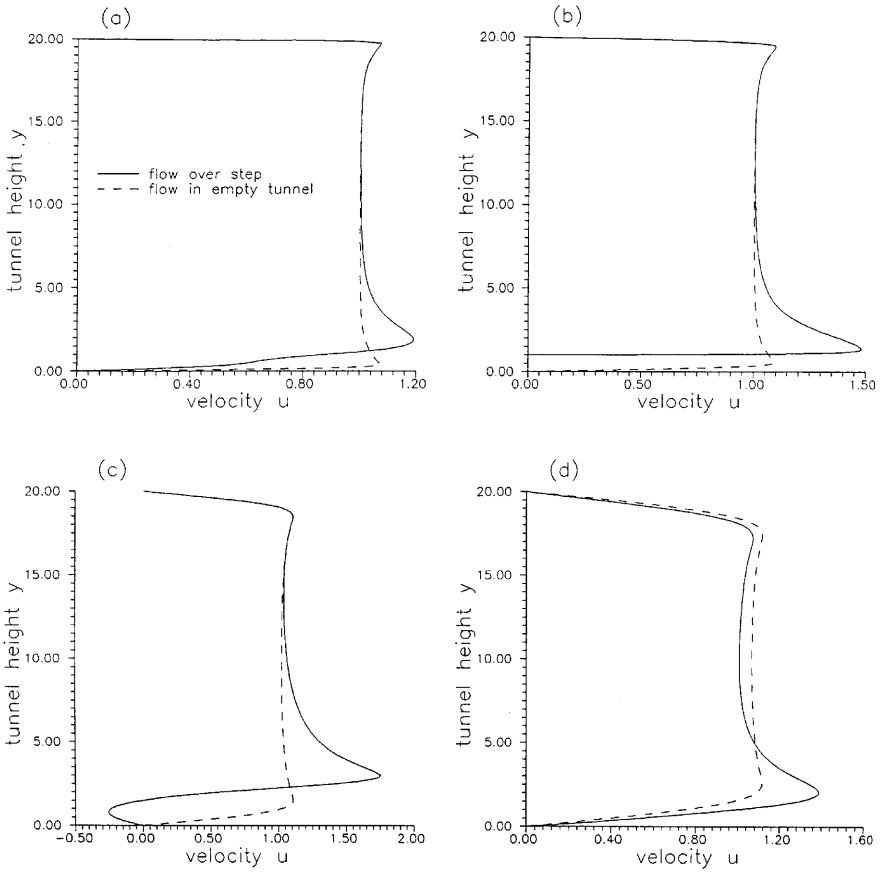

Figure 11. Typical u-velocity profiles at $Re = 70$ along tunnel with and without presence of step: (a) $x = 0{\cdot}5$; (b) $x = 1$; (c) $x = 7{\cdot}5$; (d) $x = 23$

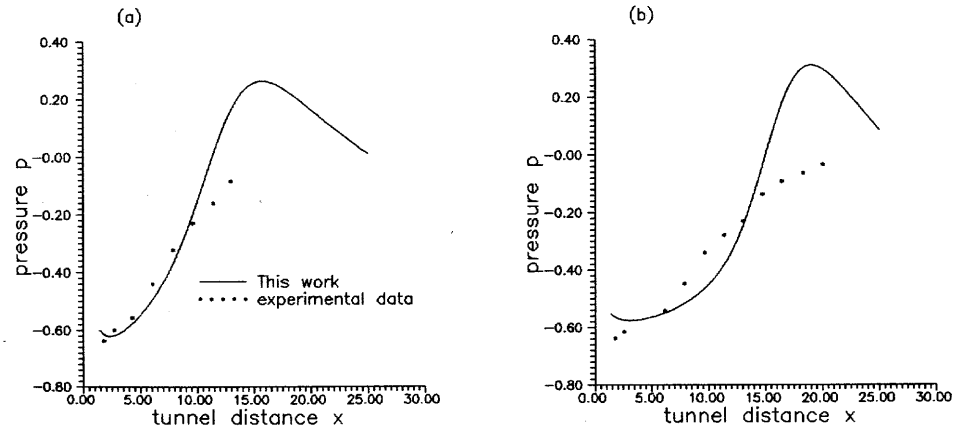

Figure 12. Comparison of numerical predictions of this work with experimental data of Acrivos *et al.* for pressure distribution downstream of flow over a rectangular step at (a) $Re = 42{\cdot}5$ and (b) $Re = 61{\cdot}9$

 © 1997 by John Wiley & Sons, Ltd.

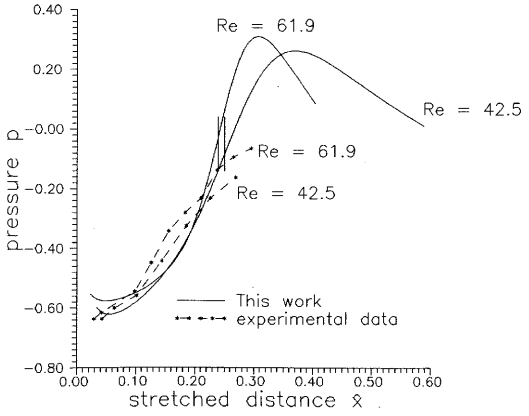

Figure 13. Comparison of numerical predictions of this work with experimental data of Acrivos *et al.* for pressure distribution downstream of flow over a rectangular step at $Re = 42{\cdot}5$ and $61{\cdot}9$ as a function of stretched coordinate $\hat{x} = x/Re$

showing that the aspect ratio 1:20 chosen for the numerical and physical experiments does not disturb the flow far away from the top of the step.

The pressure distributions are depicted in Figures 12 and 13. It is shown that the dimensionless pressure is almost independent of the Reynolds number at the corner of the step and the pressure gradient is nearly constant along the major portion of the recirculation region. The discrepancy between the numerical predictions and the experimental data is close to 10% at $Re = 42{\cdot}5$ and 20% at $Re = 61{\cdot}9$ in the wake. This relatively high discrepancy is most probably related to the inaccuracy in the pressure measurement, as stated by Acrivos *et al.* (Reference 26, p. 40, lines 8–12), due to the height of the step. In their work they also observed that by plotting the pressure versus a stretched co-ordinate $\hat{x} = x/Re$ the pressure variation should be independent of the Reynolds number. They also developed a theory for that phenomenon especially applicable to the separated flow past a circular cylinder.[35] In Figure 13 the numerical results for the pressure are shown as a function of the stretched co-ordinate $\hat{x} = x/Re$ along with the experimental data of Acrivos *et al.*, where indeed their theory is verified for the pressure distribution inside the recirculation region and the inconsistency of their model, as they state (Reference 35, p. 747), is also revealed in the region outside the wake, where the discrepancy in the pressure for the two different Reynolds numbers increases.

Based on the agreement of the numerical computations with actual experimental data, predictions were made at higher Reynolds numbers with the computational mesh of Figure 2. The results of the numerical experiments are shown in Figure 14. The recirculation region increases with increasing Reynolds number as observed earlier in the simulation of Acrivos *et al.*'s experiments in Figure 9. In fact, the length of the recirculation region is 30 times greater than the actual height of the obstacle. The calculations were stopped at $Re = 275$, since the primary interest was the estimation of the length of the recirculation region. In order to make predictions at even higher Reynolds numbers, a longer computational domain is needed, which is beyond the scope of this investigation.

In order to study the flow phenomena around the obstacle at higher Reynolds numbers by ignoring the length of the recirculation region, the computational domain must be placed in the development of the recirculation region. The issue of the appropriate outflow boundary condition arises then[14,21] and the free boundary condition is used for the first time in this problem to enable predictions at high Reynolds numbers with reasonable computational cost.

The first computer run was the Stokes flow of Figure 4 using the computational mesh of Figure 2, where the length of the computational domain was cut in the middle of the width of the channel at 5·5

© 1997 by John Wiley & Sons, Ltd.

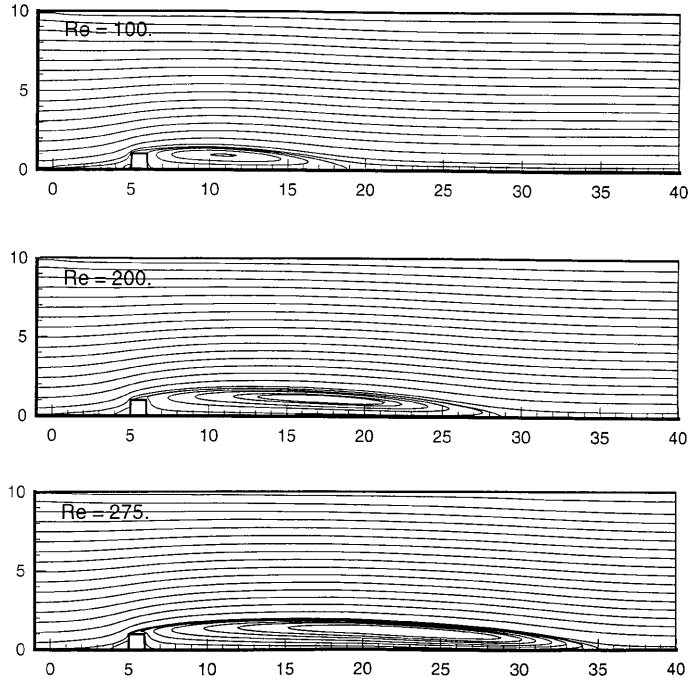

Figure 14. Numerical predictions of streamline patterns for flow over a square step at $100 \leqslant Re \leqslant 275$

and all other flow conditions were kept the same. The results of the streamlines, vorticity contours and isobars are shown in Figure 15. Comparing the results of the 'long' domain of Figures 4(a) and 6 with those of the 'short' domain of Figure 15.* there is only a slight distortion in the calculations at the exit of the 'short' domain, which is explained by the deviation of the u-velocity profile of the 'short' domain from the corresponding 'correct' one of the 'long' domain as shown in Figure 16. The implementation of the free boundary condition in the limit of Stokes flow permits the fluid to exit the domain freely without any disturbance of the flow phenomena in the interior almost up to the outflow.

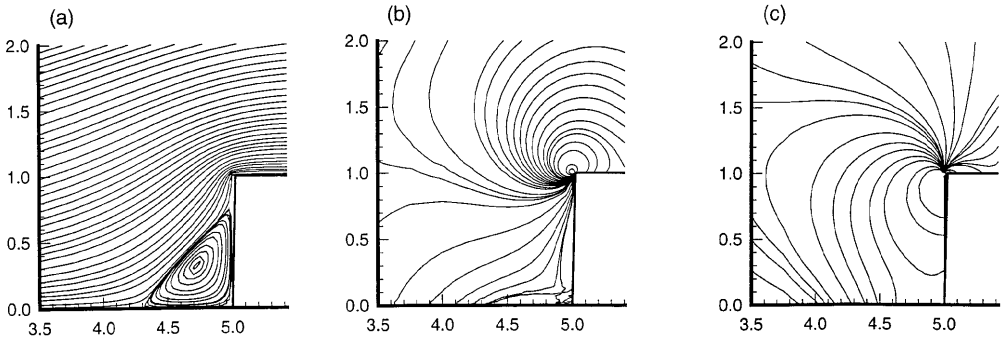

Figure 15. Predictions of (a) streamlines, (b) vorticity contours and (c) isobars in limit of Stokes flow over a square step with outflow boundary of computational domain placed in middle of width of step

* It should be noted that the number of contours is not an indication of the strength of the recirculation.

 © 1997 by John Wiley & Sons, Ltd.

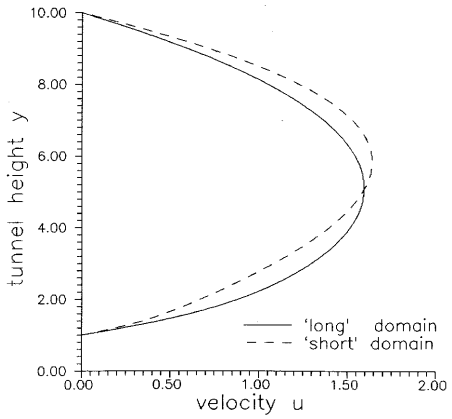

Figure 16. Comparison of u-velocity profile in 'short' and 'long' computational domains at outflow of 'short' domain in limit of Stokes flow over a square step

Next the length of the computational domain of the mesh of Figure 2 was cut at $x = 13$. Zeroth-order continuation was used from $Re = 0{\cdot}02$ to reach $Re = 275$, with intermediate Reynolds numbers 0·1, 1, 10 and 25 and then Re increased in steps of 25 up to 275. The streamline pattern at $Re = 275$ for the 'short' domain is shown in Figure 17. Again, compared with the solution of the 'long' domain in Figure 14, there is only a slight distortion just at the artificial outflow boundary at $x = 13$, which is demonstrated in the minor deviation of the u-velocity profile of the 'short' domain compared with the 'correct' solution of the 'long'domain as shown in Figure 18.

The satisfactory performance of the free boundary condition in this problem motivated further computer runs up to $Re = 2500$ with the computational domain cut at length $x = 13$ in order to study in more detail the flow phenomena around the step at higher Reynolds numbers. The predicted streamline patterns for the 'short' computational domain at $x = 13$ are shown in Figure 19. With increasing Reynolds number the recirculating eddy upstream of the step increases and downstream of

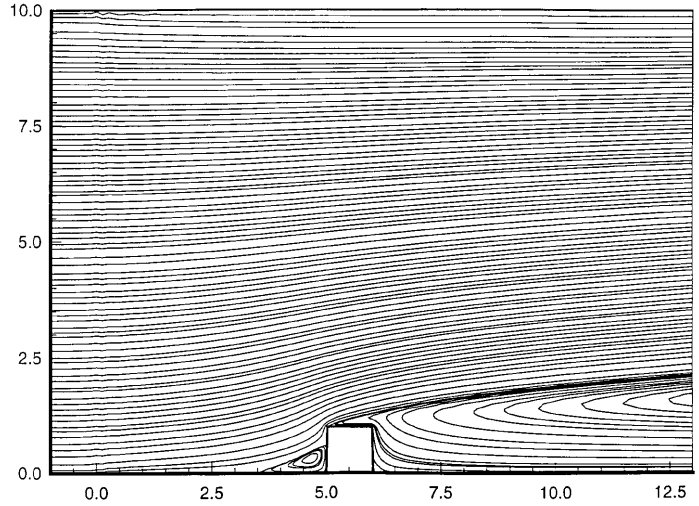

Figure 17. Numerical prediction for streamline pattern of 'short' computational domain for flow over a square step at $Re = 275$

© 1997 by John Wiley & Sons, Ltd.

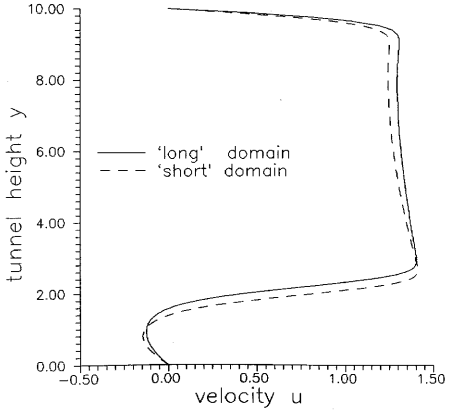

Figure 18. Comparison of u-velocity profile in 'short' and 'long' computational domains at outflow of 'short' domain for flow over a square step

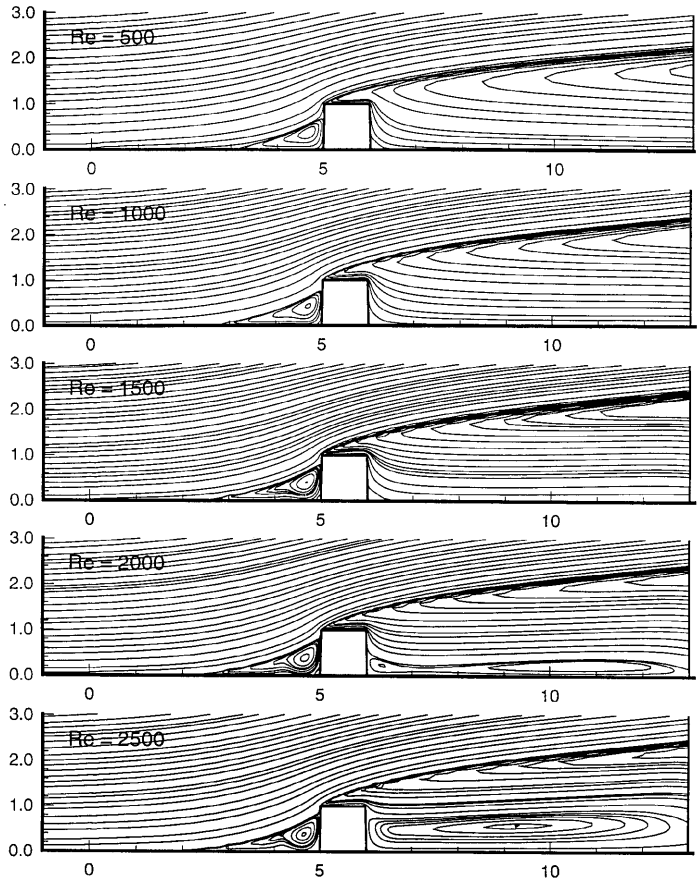

Figure 19. Numerical predictions of streamline patterns of 'short' computational domain flow over a square step at $500 \leqslant Re \leqslant 2500$

 © 1997 by John Wiley & Sons, Ltd.

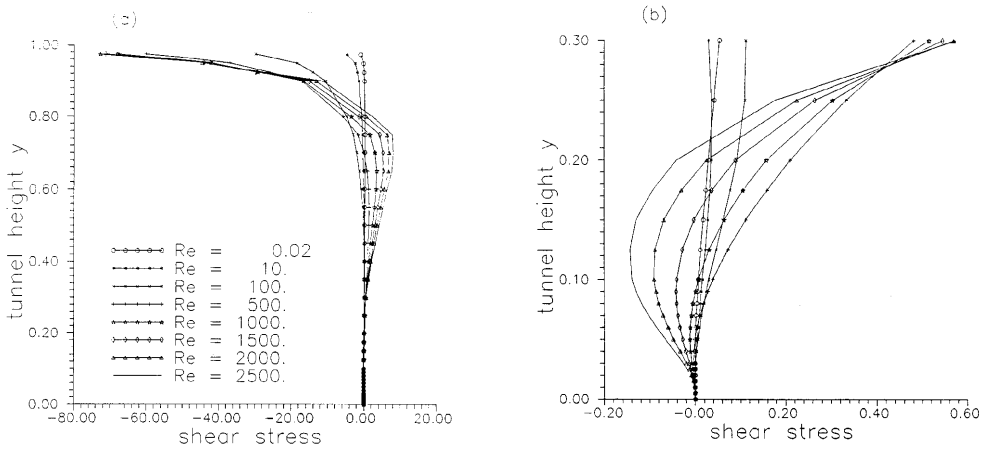

Figure 20. (a) Numerical predictions of shear stress distribution along upstream side of step for flow over a square step at $0.02 \leqslant Re \leqslant 2500$ and (b) detail of distribution

the step a secondary wake develops for $Re \geqslant 1500$. The shear stress distributions along the upstream and downstream sides of the step are shown in Figures 20 and 21 respectively. Zero shear stress is predicted at various points along the vertical sides of the step, which is compatible with kinematic studies of flows around surface-mounted obstacles reported by Hunt *et al.*,[36] who applied topology and kinematic principles for their theoretical and experimental investigations to connect the existence of attachment and reattachment points with zero shear stress. The predictions of the pressure distribution along the top of the step are shown in Figure 22. With increasing Reynolds number the so-called 'leading edge' singularity of the pressure over the step disappears owing to constant displacement of the point of separation of the flow on top of the step. The separation point has been determined, following Bradshaw,[37] by calculating the points along the sides of the obstacle where the shear stress is zero and changes sign.

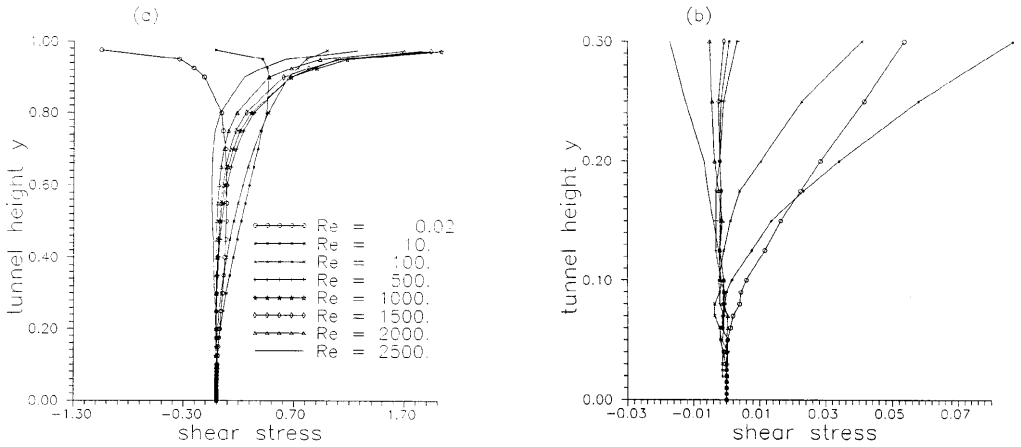

Figure 21. (a) Numerical predictions of shear stress distribution along downstream side of step for flow over a square step at $0.02 \leqslant Re \leqslant 2500$ and (b) detail of distribution

© 1997 by John Wiley & Sons, Ltd.

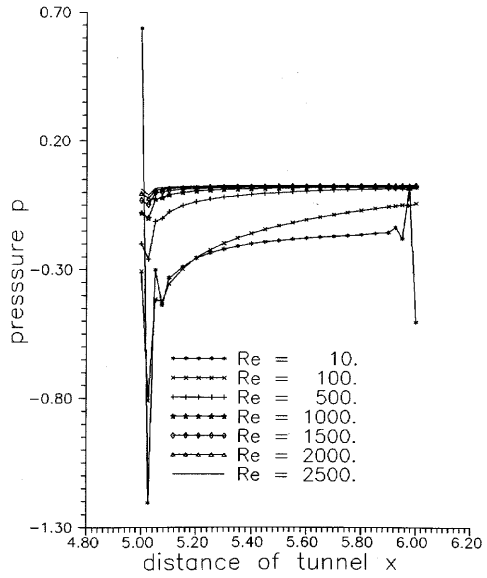

Figure 22. Numerical prediction of pressure distribution along top of step for flow over a square step at $10 \leqslant Re \leqslant 2500$

5. CONCLUSIONS

A complete model for the flow over a step has been designed, with improved inflow and outflow boundary conditions, that can simulate actual physical experiments with satisfactory accuracy. Both in the limit of Stokes flow and at Reynolds numbers up to 70, based on the height of the step, the discrepancy in the streamline pattern and the length of the recirculation region with available experimental data is less than 27% and in the pressure distribution less than 20%. Predictions for the length of the recirculation region and the shape of the streamlines are made up to $Re = 275$. The implementation of the free boundary condition at the outflow of the computational domain, where the wake is cut in its development, shows that the fluid leaves the flow domain undisturbed, so that the study of the flow phenomena around the step is permitted for higher Reynolds numbers up to 2500. It is predicted that a secondary eddy is formed downstream of the step, the leading edge singularity in the pressure distribution disappears and the shear stress along the vertical sides of the step changes sign owing to the existence of reattachment points.

The results of this work should be useful to workers who perform physical experiments in the design of wind tunnels, since issues such as the proper aspect ratio of the height of the tunnel to the height of the step and of the length of the tunnel with respect to the recirculation length are accurately examined. The analysis can be extended to the turbulent flow regime either by applying direct numerical simulation or by using appropriate turbulence closure models based on the computational model of this work.

After the establishment of the conventional Galerkin finite element method by Leone and Gresho[24] in the calculation of the complex flow phenomena of the flow over a step, this work complements their contribution by mesh refinements and improved upstream and outflow boundary conditions and represents the most accurate results for this problem in the laminar flow regime, as demonstrated in comparison with available experimental data.

 © 1997 by John Wiley & Sons, Ltd.

ACKNOWLEDGEMENTS

N.A.M. wishes to thank Professor J. Vassalos, director of the Research Institute of Chemical Processes of Thessaloniki, Greece, for the financial support of this project through a scholarship established for the continuation of the work of the late Professor Papanastasiou. The constant support of Professor S. G. Nychas and Dr. J. Papaspyros throughout this work is appreciated. S.P.P. wishes to thank Professor G. Terzides for his support. We would like to thank Dipl.-Math. T. Georgiou of Arithmotechniki Ltd. and Professor D. Diamantides of the Democritus University of Thrace for permission to run our programmes on their computing facilities.

REFERENCES

1. P. K. Yeung and S. C. Kot, 'Computation of turbulent flows past arbitrary two-dimensional surface-mounted obstructions', *J. Wind Eng. Ind. Aerodyn.*, **18**, 177–190 (1985).
2. C. P. Crosby, E. H. Matthews and J. P. du Plessis, 'The numerical prediction of airflow through and around permeable windbreaks and over buildings', in C. Taylor, P. Gresho, R. L. Sani and J. Hauser (eds), *Numerical Methods in Laminar and Turbulent Flows*, Pineridge, Swansea, 1989, pp. 643–653.
3. R. R. Hwang and Y. F. Peng, 'Computation of backward-facing step flows by a second-order Reynolds stress closure model', *Int. j. numer. methods fluids*, **21**, 223–235 (1995).
4. E. Le Huu Nho and C. Beguier, 'Three dimensional hot wire measurements behind a swept backward facing step', in R. Benzi (ed.), *Advances in Turbulence V*, Kluwer, Dordrecht, 1995, pp. 303–307.
5. Y.-J. Hong, S.-S. Hsieh and H.J. Shih, 'Numerical computation of laminar separation and reattachment of flow over surface mounted ribs', *Trans. ASME, J. Fluids Eng.*, **113**, 190–198 (1991).
6. J. P. Glekas and G. C. Bergeles, 'Dispersion under neutral atmospheric conditions', *Int. j. numer. methods fluids*, **19**, 237–257 (1994).
7. N. Toy and K. Ainkaran, 'An experimental and numerical investigation of separated and reattched flows', in C. Taylor, W. G. Habashi and M. M. Hafez (eds), *Numerical Methods in Laminar and Turbulent Flows*, Pineridge, Swansea, 1987, pp. 572–583.
8. D. T. Valentine and G. W. Hyde, 'Axisymmetric laminar flow over an annular backstep: a numerical study', in C. Taylor, W. G. Habashi and M. M. Hafez (eds), *Numerical Methods in Laminar and Turbulent Flows*, Pineridge, Swansea, 1987, pp. 607–618.
9. J. S. Dekruif and A. A. Hassan, 'Implications of truncating semi-infinite physical domains on the accuracy of the solutions to the N–S equations', *Int. j. numer. methods fluids*, **8**, 133–146 (1988).
10. E. Dick, 'A partial flux-splitting method for steady incompressible Navier–Stokes equations', in C. Taylor, W. G. Habashi and M. M. Hafez (eds), *Numerical Methods in Laminar and Turbulent Flows*, Pineridge, Swansea, 1987, pp. 549–559.
11. P. G. Pattani and M. D. Olson, 'Finite element algebraic closure modelling of turbulent entrance type flows', in C. Taylor, W. G. Habashi and M. M. Hafez (eds), *Numerical Methods in Laminar and Turbulent Flows*, Pineridge, Swansea, 1987, pp. 386–397.
12. D. K. Gartling, 'A test problem for outflow boundary conditions—flow over a backward-facing step', *Int. j. numer. methods fluids*, **11**, 953–967 (1990).
13. T. C. Papanastasiou, N. Malamataris and K. Ellwood, 'A new outflow boundary condition', *Int. j. numer. methods fluids*, **14**, 587–608 (1992).
14. R. L. Sani and P. M. Gresho, 'Résumé and remarks on the open boundary condition minisymposium', *Int. j. numer. methods fluids*, **18**, 983–1008 (1994).
15. P. M. Gresho, D. K. Gartling, J. R. Torczynski, K. A. Cliffe, K. H. Winters, T. J. Garratt, A. Spence and J. W. Goodrich, 'Is the steady viscous incompressible two-dimensional flow over a backward-facing step at $Re = 800$ stable?', *Int. j. numer. methods fluids*, **17**, 501–541 (1993).
16. S. Murakami and A. Mochida, 'Three-dimensional numerical simulation of turbulent flow around buildings using the k–ε turbulence model', *Bld. Environ.*, **24**, 51–64 (1989).
17. D. Burry, G. Papadakis and G. Bergeles, 'Numerical prediction of three dimensional turbulent flow and pollutant dispersion around a cube', *Proc. Florence World Energy Research Symp.*, Florence, July 1994, pp. 855–863.
18. R. W. Benodekar, A. J. H. Goodard, A. D. Gosman and R. I. Issa. 'Numerical properties of turbulent flow over surface-mounted ribs', *AIAA J.*, **23**, 359–366 (1985).
19. Y. G. Chan, 'Numerical solution of the two dimensional incompressible separated flow' in C. Taylor, W. G. Habashi and M. M. Hafez (eds), *Numerical Methods in Laminar and Turbulent Flows*, Pineridge, Swansea, 1987, pp. 749–759.
20. F. Durst and A. K. Rastogi, 'Theoretical and experimental investigations of turbulent flows with separation', *Proc. Symp. on Turbulent Shear Flows*, University Park, PA, April 1977, Vol. 1.
21. P. M. Gresho, 'Incompressible fluid dynamics: some fundamental formulation issues', *Ann Rev. Fluid Mech.*, **23**, 413–453 (1991).

© 1997 by John Wiley & Sons, Ltd.

22. D. Greenspan, 'Numerical studies of steady, viscous, incompressible flow in a channel with a step', *J. Eng. Math.*, **3**, 21–28 (1969).
23. M. Friedman, 'Laminar flow in a channel with a step', *J. Eng. Math.*, **6**, 285–290 (1972).
24. J. M. Leone and P. M. Gresho, 'Finite element simulation of steady, two-dimensional, viscous incompressible flow over a step', *J. Comput. Phys.*, **41**, 167–191 (1981).
25. S. Taneda, 'Visualization of separating Stokes flows', *J. Phys. Soc. Jpn.*, **46**, 1935–1942 (1979).
26. A. Acrivos, L. G. Leal, D. D. Snowden and F. Pan, 'Further experiments on steady separated flows past bluff objects', *J. Fluid Mech.*, **34**, 25–48 (1968).
27. N. Malamataris and T. C. Papanastasiou, 'Unsteady free surface flows on truncated domains', *Ind. Eng. Chem. Res.*, **30**, 2211–2219 (1991).
28. N. Malamataris, 'Computer-Aided Analysis of Flows on Moving and Unbounded domains: phase-change fronts and liquid leveling', *Ph.D. Thesis*, University of Michigan, Ann Arbor, MI, 1991.
29. J. C. Heinrich and C. A. Vionnet, 'On boundary conditions for unbounded flows', *Commun. numer. methods eng.*, **11**, 179–185 (1995).
30. D. F. Griffiths 'The ''No Boundary Condition'' Outflow Boundary Condition', *Int. j. numer. methods fluids*, **24**, 393–411 (1997).
31. M. Renardy 'Imposing ''No'' Boundary Condition at Outflow: Why Does it Work?', *Int. j. numer. methods fluids*, **24**, 413–417 (1977).
32. V. P. Fragos, 'Computer-aided analysis of flow over a surface mounted obstacle', *M.Sc. Thesis*, Aristotle University of Thessaloniki, 1995.
33. P. Hood, 'Frontal solution program for unsymmetric matrices', *Int. j. numer. methods eng.*, **10**, 379 (1974).
34. R. L. Panton, *Incompressible Flow*, Wiley, New York, 1984.
35. A. Acrivos, D. D. Snowden, A. S. Grove and E. E. Peterson, 'The steady separated flow past a circular cylinder at large Reynolds numbers', *J. Fluid Mech.*, **21**, 737–760 (1965).
36. R. C. J. Hunt, J. C. Abell, A. J. Peterka and H. Woo, 'Kinematical studies of the flow around free- or surface-mounted obstacles; applying topology to flow visualization', *J. Fluid Mech.*, **86**, 179–200 (1978).
37. P. Bradshaw, *Experimental Fluid Mechanics*, Pergamon/Macmillan, New York, 1964.

 © 1997 by John Wiley & Sons, Ltd.